ACS OMEGA

http://pubs.acs.org/journal/acsodf

Article

Sorption of Carbon Dioxide and Nitrogen on Porous Hyper-Cross-Linked Aromatic Polymers: Effect of Textural Properties, Composition, and Electrostatic Interactions

Noufal Merukan Chola,[‖] Prayag Gajera,[‖] Harshal Kulkarni,[‖] Gaurav Kumar, Rahulbhai Parmar, Rajaram K. Nagarale,* and Govind Sethia*

Cite This: *ACS Omega* 2023, 8, 24761−24772

Read Online

ACCESS | Metrics & More | Article Recommendations | Supporting Information

ABSTRACT: Porous hyper-cross-linked aromatic polymers are one of the emerging classes of porous organic polymers with the potential for industrial application. Four different porous polymeric materials have been prepared using different precursors (indole, pyrene, carbazole, and naphthalene), and the composition and textural properties were analyzed. The materials were characterized in detail using different physicochemical techniques like scanning electron microscopy, transmission electron microscopy, nitrogen adsorption at 77 K, Fourier transform infrared spectroscopy, X-ray diffraction, etc. The effect of textural properties and nitrogen species on carbon dioxide and nitrogen adsorption capacities and selectivity was studied and discussed. The carbon dioxide and nitrogen adsorption capacities were measured using a volumetric gas adsorption system. The adsorption data were fitted into different adsorption models, and the ideal absorbed solution theory was used to calculate adsorption selectivity. Among the studied samples, POP-4 shows the highest carbon dioxide and nitrogen adsorption capacities. While POP-1 shows maximum CO_2/N_2 selectivity of 78.0 at 298 K and 1 bar pressure. It is observed that ultra-micropores, which are present in the prepared materials but not measured during conventional surface area measurement via nitrogen adsorption at 77 K, play a very important role in carbon dioxide adsorption capacity and determining the carbon dioxide selectivity over nitrogen. Surface nitrogen also increases the CO_2 selectivity in the dual mode by increasing carbon dioxide adsorption via the acid−base interaction as well as by decreasing nitrogen adsorption due to N−N repulsion.

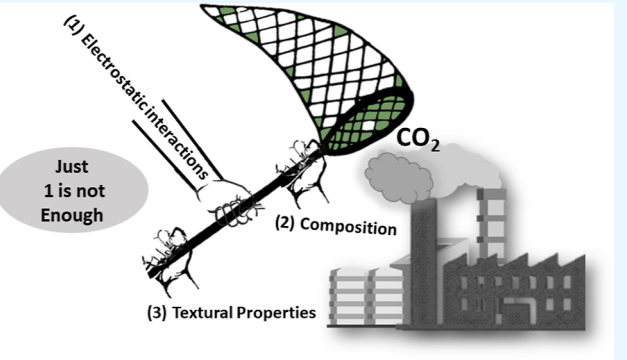

1. INTRODUCTION

The increasing use of fossil fuels not only caused air and water pollution but also led to enormous CO_2 emissions into the environment. The CO_2 concentration in the environment reached 420.95 ppm from 280 ppm in the pre-industrial revolution.[1] This alarming increase in CO_2 is resulting in a destructive effect on the environment, climate change, and global warming. Different gas molecules like carbon dioxide, water vapor, methane, and ozone are mainly responsible for the greenhouse effect. However, among the anthropogenic greenhouse gases, CO_2 contributes more than 60% to total global warming because of its huge emission amount.[2] Among the total anthropogenic carbon dioxide emissions, approximately 30% of the carbon dioxide released into the environment comes from fossil fuel-based power plants, which are the main contributors to climate change.[3] The efficient mitigation of CO_2 emissions from large point sources, like power plants, has gained significant attention.[4,5] The development of technology to decrease the emission of carbon dioxide via capture, storage, or utilization of carbon dioxide has attracted huge attention in the past few decades, and it is now considered a basic requirement for the continued growth and development of society without causing harm to the environment. Globally, extensive efforts are underway to develop efficient and economic solutions for carbon dioxide capture and utilization.[5] The development of suitable adsorbents and economic processes for the separation of carbon dioxide from its mixture with nitrogen is the key requirement for the success of carbon capture and utilization technologies. Many adsorbents belonging to different classes of materials, like organic, inorganic, and hybrid materials, have been developed for CO_2 capture.[5] For effective and economic carbon dioxide capture, an adsorbent should have high adsorption capacity, selectivity, kinetics, and stability under harsh flue gas

Received: November 25, 2022
Accepted: May 24, 2023
Published: July 6, 2023

conditions and toward impurities.[6] Despite a variety of porous adsorbents like MOFs,[7] zeolites,[8] clay[9] carbons,[10] mesoporous silicas,[11] graphene, composite materials,[12] and polymers,[13] it remains challenging to develop a material to have all the critical adsorbent requirements like CO_2 adsorption capacity, selectivity, chemical, thermal stability, fast kinetics, recyclability, low energy consumption, low material cost, and mechanical robustness.

The development of materials with tuned porosity and composition is very important for CO_2 capture.[5,14−16] Among the different classes of adsorbents, microporous materials are considered the most promising and potential adsorbents for CO_2 separation. Porous organic polymer materials are one of the most promising emerging materials for CO_2 capture due to their high porosity, carbon dioxide adsorption capacity, adsorption selectivity, simple synthesis procedure, and low cost.[5,17] The porous materials can be further modified by nitrogen-containing functionalities for enhanced CO_2 capture.[18] A large number of porous polymer-based adsorbents have been developed for CO_2 capture.[19,20] Among different microporous adsorbents, the porous organic polymer has few advantages over other microporous adsorbents. However, the CO_2 adsorption capacities for porous polymer-based adsorbents are still somewhat low as compared with the best MOFs but can be partly balanced by their higher chemical and thermal stabilities and their less hydrophilic nature.[20−22] Moreover, the porous polymers had the potential for commercial applications owing to their excellent chemical, thermal, and structural stability under flue gas conditions. Although having advantages over the other materials, the POP material usually presents low CO_2 capture and CO_2/N_2 selectivity in comparison with other porous materials due to a lack of suitable pore structure tuning, functionalization, and low affinity for CO_2, which retards their practical applications. The development of POPs with a higher surface area and tuned micro-porosity and functionalization is considered an important parameter for increasing the adsorption capacity and selectivity of the materials.[20,23]

POPs were reported, which are derived from organic molecules as precursors. They have been named according to the method of their preparation. Covalent organic frameworks (COF, which are mostly crystalline), porous aromatic frameworks (PAF, mostly amorphous), and conjugated microporous polymers are some of the most extensively studied classes of porous polymers.[22,24] The first pioneering work on COF was reported by Yaghi et al. in 2005, after which numerous reports have flourished on this class of polymers for diverse applications.[25] Cyanuric chloride-derived COFs were named covalent triazine-based frameworks, which are mostly crystalline polymers with peculiar properties for selective gas adsorption.[26] Because of the inherent polar characteristic of the C═N bond in the polymer, the adsorption selectivity toward CO_2 molecules has been well explored. A remarkable advantage of POPs over other inorganic-based adsorbents is that wise molecular engineering is possible to achieve the desired property. The pore size, uniformity, and homogeneity of the pores, electrophilicity/electrophobicity, and polarity non-polarity of the polymers would be dependent on the starting precursors as well as the method of preparation. It is also found that the introduction of the heteroatom would endow the polymer with much more polarity, which would lead to selective gas adsorption capacity.[27]

Among the broad pore size distribution (PSD) of porous adsorbent materials, pores less than 1 nm are mainly responsible for CO_2 capture. Several researchers reported the importance of small micropores (<1 nm) for CO_2 adsorption.[10,22,28] Sethia and Sayari[10] showed that CO_2 capture under ambient conditions depends on the volume of micropores having a diameter smaller than 0.8 nm, and the critical role of micropores depends on the adsorption conditions. Particularly, temperature and the mechanism of adsorption. Considering the importance of textural properties and getting insight from the various reports showing the importance of micropore diameter, we successfully prepared microporous porous organic polymer materials with high surface area and micropore volume.

Porous polymer materials are widely used for gas separation applications in membranes. However, their application as adsorbent materials in pressure swing adsorption based gas separation is not explored in detail. The possible use of POP as an adsorbent for gas separation and CO_2 capture is now getting huge attention. Here, we have developed a low-cost microporous organic polymer via a simple synthesis protocol without using noble metals and with decent CO_2 adsorption capacity and CO_2/N_2 selectivity without functionalization. We followed a special "knitting type" polymerization in which dimethoxy methane was used as the knitting agent with various aromatic precursors. The reaction proceeded with a Friedel−Crafts-type $FeCl_3$-catalyzed one-pot reaction under reflux conditions. Aromatic rings would be dominantly present in the polymer products due to the huge molecular size difference with the methylene bridge.[29] The striking advantage of this class of polymers is that the aromatic rings possess amazing flexibility, regardless of the precursors, and the methylene bridge can be the deciding factor in this bond flexibility. The prime motive for choosing knitting-type polymerization is the flexibility between the monomer rings that determine the porosity of the material. Compared to the graphitic-type materials, the rings are fused, so stereochemical ring flipping is not possible. Whereas the materials with flexibility in the rings can have the maximum possible spatial arrangements in the rings, which create porosity in the material.[30] With this work, we believe that the flexibility of the aromatic rings would greatly influence the selectivity of the gas separation. The developed materials can be further functionalized for higher carbon dioxide adsorption capacity and selectivity.[31] The effect of pore diameter on the carbon dioxide and nitrogen adsorption properties of the materials was also studied and discussed.

In the case of MOFs, the metal precursors as well as the precise organic ligands are very crucial for a better result. Also, they have been extensively explored for adsorption studies. Our intention with this study was to explore a metal-free system with relatively low-cost precursors to achieve higher efficiency. As these materials are metal-free, they are easy to dispose of. Also, these materials are economical, unlike MOFs, which generally require hazardous and expensive chemicals and stringent reaction conditions. Knitted COF polymers are less explored, to the best of our knowledge, and they may be promisingly better adsorbents for controlled gas adsorption storage and release. The study is carried out to gain a general understanding of the pure hydrocarbon-based COF and the effect of nitrogen loading. These starting precursors are relatively low-cost and readily available, and therefore, the possibility of scaling up such material is also remarkably noticed.

https://doi.org/10.1021/acsomega.2c07553
ACS Omega 2023, 8, 24761−24772

Scheme 1. General Synthesis of the "Knitting Type" Naphthalene-Based Hyperbranched Cross Linked Polymer

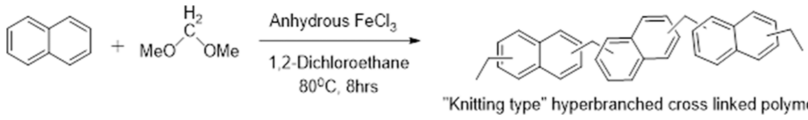

The majority of work on carbon dioxide and nitrogen adsorption on porous materials primarily focuses on the textural properties, like surface area and pore diameter, of the adsorbent rather than electrostatic interaction between the adsorbent and gas molecules.[2,10,15,23,28] At the same time, carbon dioxide adsorption became the primary focus. Though nitrogen adsorption also equally determines the adsorption selectivity and overall performance of the adsorbents. The role of acid−base interactions and the effect of the N-hetero atom on the adsorption behavior of adsorbents have been extensively reported in the literature.[16,31−33,41] However, very few reports are available regarding the N−N interaction between N-adsorbate and nitrogen molecules; a more detailed investigation is required to investigate the role of N−N interactions.[34−36] In the present manuscript, we discussed both carbon dioxide and nitrogen adsorption, considering possible electrostatic interactions like acid−base interaction and N−N repulsion with the textural properties of the material.

2. MATERIAL AND METHODS

2.1. Materials. Anhydrous $FeCl_3$ was obtained from Sigma-Aldrich; dimethoxymethane and biphenyl were purchased from Alfa, and anhydrous dichloroethane was obtained from Thermo Fisher. All chemicals have been used as such without further purification.

2.2. Methods. To a solution of indole (20 mmol) and dimethoxymethane (40 mmol) in 1,2-dichloroethane (30 mL) anhydrous ferric chloride (40 mmol), equivalent to the knitting reagent (dimethoxymethane), was added under nitrogen flow (Scheme 1). The nitrogen flow was allowed for 30 min, and the reaction was left to heat at 80 °C for 12 h. The crude solid was filtered and washed with methanol, de-ionized water, and 2 M HCl several times and vacuum dried (yield ∼92%). The same synthetic procedure was followed for the preparation of the rest of the polymers, yielding ∼91% carbazole, ∼95% naphthalene, and ∼96% pyrene. The slight variation in yield is due to the different reactivity, which depends on the aromaticity of the precursors used. Indole, pyrene, carbazole, and naphthalene-derived porous polymer samples were named POP-1, POP-2, POP-3, and POP-4, respectively.

The effect of exposure to steam, carbon dioxide, and air on the carbon dioxide adsorption capacity of porous polymer samples was investigated. In a typical run, the sample was treated under flowing carbon dioxide, air, and steam for 8 h using a fixed-bed column maintained at 120 °C. The carbon dioxide adsorption isotherm for the material was measured before and after the treatment. A schematic diagram (Figure S1) for the experimental set-up used and the adsorption/desorption isotherm before and after treatment (Figure S2) are given in Supporting Information.

2.3. General Characterization. The Fourier transform infrared spectroscopy (FTIR) spectra were recorded with a PerkinElmer (Germany) GXFTIR system in the 400−4000 cm^{-1} range. The XRD diffraction patterns were recorded with a PAN Analytical (Germany) system using the Cu Kα line (λ = 1.5406 Å) between 2 and 60°. The surface morphology was visualized using a JSM-7100F, Japan field emission scanning electron microscope equipped with an energy-dispersive X-ray detector (EDX). The thermogravimetric analysis was performed at a heating rate of 10 °C min^{-1} from room temperature to 800 °C in the air. High-resolution transmission electron microscopy (HRTEM; FEI Tecnai G2 12 Twin) was performed at 120 kV. Raman spectroscopy (Model: Alpha, Make: WITec, Germany) was performed in the 400−3000 cm^{-1} frequency range with a 514 nm laser source.

2.4. Material Characterizations. The FTIR characterization of each material was performed and analyzed as follows. Aromatic C−H stretch was observed in ∼3030 cm^{-1}, and other aromatic peaks were identified as ∼1614 cm^{-1} for C=C bending, ∼1400, and ∼735 cm^{-1} for C−C bending and out of the plane bend in C−H aromatics, respectively, ∼1433 cm^{-1} for the C−H bend, 1323 and ∼884 cm^{-1} for C−H rock, and 2864, 2925, and 2962 cm^{-1} for C−H stretch in the methylene group.[37] Thus, the presence of knitting type CH_2 in the polymer was confirmed by C−H signals that appeared in the infrared spectra, as highlighted in Figure 1A. XRD pattern has

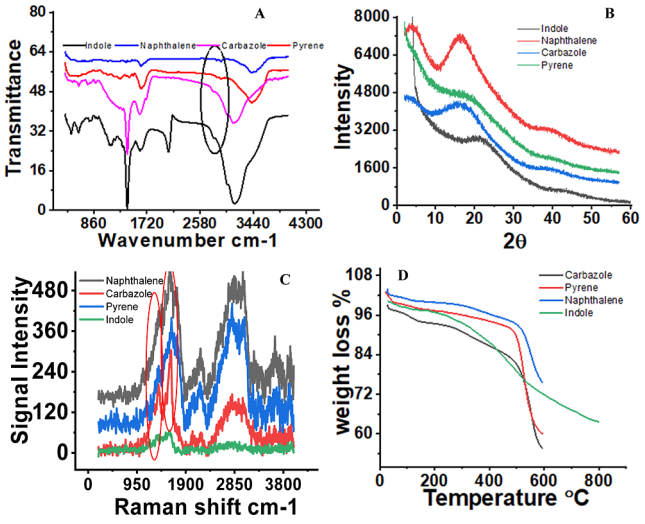

Figure 1. (A) FTIR, (B) powder XRD, (C) Raman spectra, and (D) TGA of the synthesized polymers.

also been shown in Figure 1B, the amorphous nature of the material was observed from the spectrum. Two very clear, broad peaks have been observed. The peaks observed at a 2θ value of ∼44° corresponded to 100 crystallographic planes, which indicates a honeycomb-type low ordered graphitic structure.[38] Also, the peak observed at ∼21°, which belongs to the 002 planes, is attributed to the consistent parallel stacking domains of the graphene-type 2D layered sheets.[39] These peaks confirmed that the synthesized porous hyper-cross-linked aromatic polymers (PHAPs) possess graphitic-type layered structures. The interlayer spacing was calculated by the Braggs equation, which is $2d \sin\theta = \lambda$, where d corresponds to the interlayer spacing, θ is the diffraction angle, and λ indicates the X-ray wavelength, which is 1.5 Å. The d value was

https://doi.org/10.1021/acsomega.2c07553
ACS Omega 2023, 8, 24761−24772

calculated by considering the reflections from the crystallographic plane 001 at $2\theta = \sim 7°$. From the peaks observed in the XRD spectrum, a clear peak was observed for PHAPs derived from naphthalene, which was found to be diminished in the case of other polymer samples. The interlayer spacing was calculated to be 2.142 nm, which is higher than that of the typical graphene oxide layers. Raman spectral analysis also has been carried out as represented in Figure 1C. Two characteristic bands were observed at ~1351 cm^{-1}, which also clearly indicates the graphitic disorder structure and "G" bands at ~1593 cm^{-1}, which is attributed to the sp^2 hybrid carbons in two-dimensional hexagonal lattices.[40] Very strong bands appeared at ~2790 cm^{-1}, denoted as "2D", which was attributed to the graphitic type sp^2 hybrid carbon materials by a process called second-order phonon excitations, which is mainly observed by the multi-layer 2D type graphitic materials. Further, the thermal stability of PHAPs has been analyzed by TGA, as shown in Figure 1D. The thermal stability of the naphthalene-derived PHAPs was found to be very promising compared to the other polymers. It was found that 2% of the weight loss occurred over 320 °C, and 93% of the material was retained even after 500 °C after which a drastic decrease in weight loss was observed. Generally, we found that the synthesized PHAPs have outstanding thermal stability, rendering them very promising for high-temperature applications. Electron microscopic images were also taken for the surface morphology and topology of the PHAPs. Interestingly, from FESEM images, it was found that naphthalene-derived polymers possess hollow spheres, which helped substantially increase the surface area of the material. For the pyrene-derived sample, we could observe the hollow semi-spheres, as shown in Figure 2. It was assumed that the aromatic fused ring

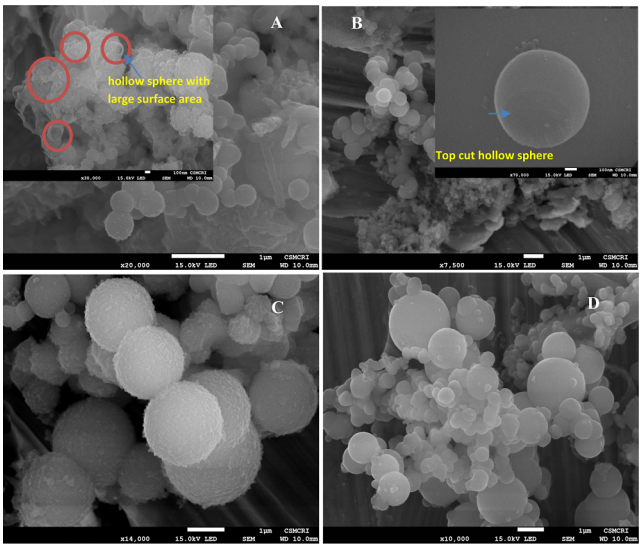

Figure 2. FESEM images of (A) naphthalene (scale bar 100 nm in set), (B) pyrene (scale bar 100 nm in set), (C) carbazole, and (D) indole.

system helped the polymer possess such a peculiar morphology which could not be observed in other polymers.[41] The composition and, particularly, the amount of nitrogen in the materials were measured using EDX measurements. Figure 3. Shows the EDX spectra for POP-1 and POP-3. The EDX spectra indicated the presence of nitrogen in POP-1 and POP-3. The relative atomic % of elements in the materials based on EDX measurements is given in Table S1. TEM images have also been taken for naphthalene-derived polymers, as shown in Figure 4. The layered porous structures have been observed from the images,

confirming further the layered graphitic-type structural characteristics.

The textural properties like surface area and pore volume for the prepared samples were determined from the nitrogen adsorption isotherm generated using a surface area analyzer (Micromeritics ASAP 2020). The specific surface area of the samples was calculated using the BET equation. The adsorption data in the relative pressure (P/P_0) range of 0.002−0.3 is used for the surface area measurement. The BET consistency rules by Rouquerol[42,43] were applied to the adsorption isotherm for the BET surface area measurements. The micropore volume was determined using a *t*-plot, while the total pore volume was calculated from the amount of nitrogen adsorbed at $P/P_0 = 0.97$. The PSD was determined by the BJH (Barrett, Joyner, and Halenda) model applied to the desorption branch of the nitrogen adsorption isotherm generated at 77 K.

The carbon dioxide and nitrogen adsorption capacities, the heat of adsorption, and the adsorption selectivity were determined from the adsorption isotherms measured at 0, 15, and 25 °C. The presence of adsorbed water and other species in the porous polymer significantly affects their adsorption behavior; therefore, the porous polymer samples were activated by heating to 150 °C for 6 h at a heating rate of 5 °C min^{-1} under a high vacuum. Carbon dioxide and nitrogen adsorption isotherms were measured using a static volumetric system. A constant temperature (±0.1 °C) during the adsorption isotherm measurement was maintained by recirculating a constant-temperature water-isopropanol mixture. A calculated amount of the CO_2/N_2 gas was dosed onto the porous polymer samples kept in the sample tube, and the volume of gas required to attain the targeted pressure points was in the range of 0.01−1.1 bar. Pressure transducers of three different capacities, 1, 10, and 1000 mmHg, were used for the pressure measurements. The CO_2/N_2 equilibrium gas adsorption/desorption for each pressure point is measured with a minimum equilibrium interval of 30 s, relative target tolerance of 5%, and an absolute target tolerance of 5 mmHg. The CO_2/N_2 adsorption selectivity was measured using the ideal adsorbed solution theory (IAST). The carbon dioxide and nitrogen adsorption data were fitted to different model equations. The IAST calculations and model equation fitting were carried out using the software OriginPro v8.5. All successful model equation fittings corresponded to adjusted R^2 values of more than 0.99. Figures S3−S6 showed adsorption the isotherm and model fitting for POP-1, POP-2, POP-3, and POP-4, respectively.

Langmuir model (single-site)

$$q = \frac{q_{max} bp}{1 + bp}$$

Langmuir model (dual-site)

$$q = q_A + q_B = \frac{q_{max} b_A p}{1 + b_A p} + \frac{q_{max} b_B p}{1 + b_B p}$$

where q is the amount of gas molecules, q_{max} is the amount of gas molecules at saturation, b is the Langmuir constant, and A and B represent different adsorption sites.

https://doi.org/10.1021/acsomega.2c07553
ACS Omega 2023, 8, 24761−24772

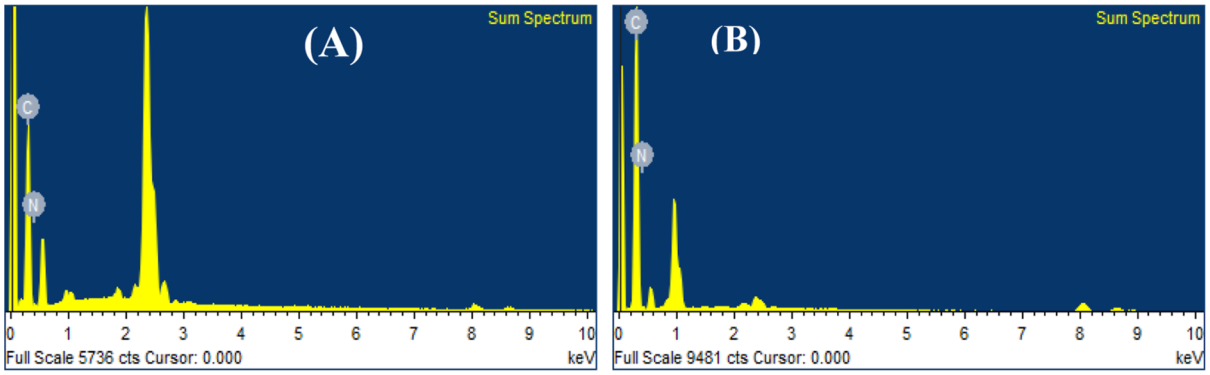

Figure 3. EDX spectra of (A) carbazole and (B) indole.

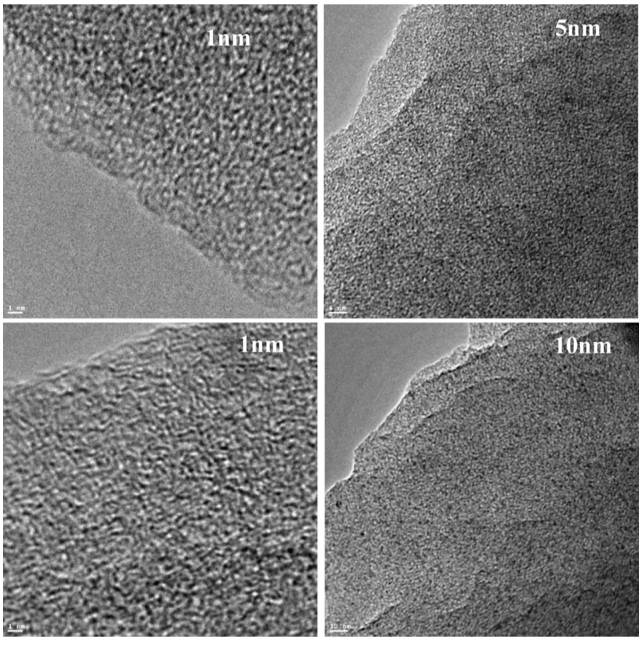

Figure 4. TEM images of naphthalene-derived COF.

The CO_2/N_2 (0.15:0.85) IAST selectivity for the gas mixture was calculated using the equation given below.

$$S = \frac{q_1/q_2}{p_1/p_2}$$

where S is the adsorption selectivity, q_1 and q_2 are the loading of gases, and p_1 and p_2 indicate the partial pressure for adsorbed gases.

3. RESULT AND DISCUSSION

The porous polymer samples were prepared using different organic molecules. The materials were thoroughly characterized using different physicochemical techniques. Carbon dioxide and nitrogen equilibrium adsorption capacities, CO_2/N_2 selectivity, and heat of adsorption were measured, and the gas adsorption capacities are discussed in relation to material composition and textural properties.

3.1. Textural Properties of the Materials. The nitrogen sorption isotherms and corresponding PSDs of porous polymer materials prepared using different precursors are displayed in Figures 5 and 6, respectively. POP-1 and POP-2 showed very low nitrogen adsorption at 77 K. However, POP-3 and POP-4

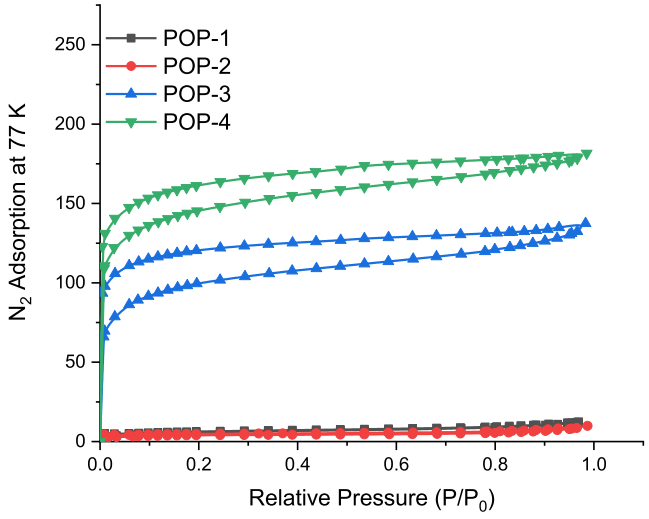

Figure 5. Nitrogen adsorption/desorption isotherm at 77 K for porous organic polymer samples.

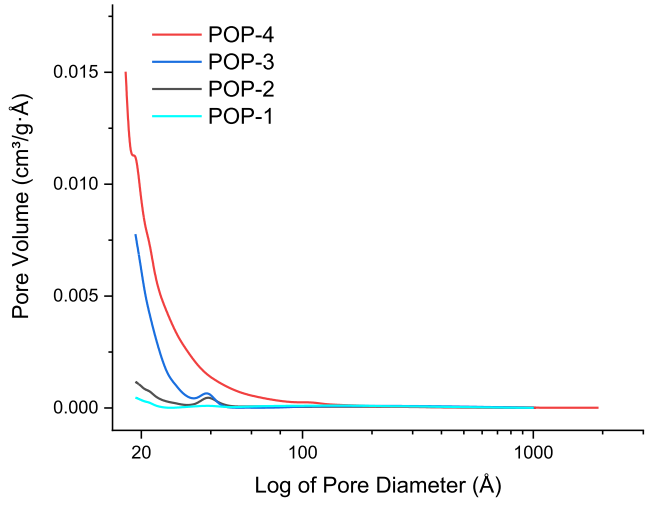

Figure 6. BJH PSD of porous organic polymer samples.

show sharp uptake at a low relative pressure ($P/P_0 < 0.1$), like a typical type-1 adsorption isotherm. High uptake at low relative pressure indicates the presence of microporosity in these materials. The changes in the shape of the PSD indicate changes in the porous structure of the materials. Indeed, BJH PSDs shown in Figure 6 corroborate and confirm the porous indication obtained from the nitrogen adsorption isotherms at

https://doi.org/10.1021/acsomega.2c07553
ACS Omega 2023, 8, 24761−24772

Table 1. Textural Properties of Porous Polymer Samples

sample code	sample precursor	BET surface area (m^2/g)	micropore surface area (m^2/g)	external surface (m^2/g)	BJH desorption (cm^3/g) pore volume				*t*-plot micropore volume (cm^3/g)	BJH desorption average pore diameter (Å)
					micro PV	meso PV	macro PV	total PV		
POP-1	indole	22	15	6	0.001	0.019	0.032	0.052	0.01	170
POP-2	pyrene	56	34.7	22.3	0.003	0.034	0.033	0.07	0.02	89.2
POP-3	carbazole	338	284	57	0.153	0.045	0.002	0.20	0.133	30.3
POP-4	naphthalene	585	497	85	0.218	0.108	0.014	0.34	0.24	28.7

Table 2. Carbon Dioxide and Nitrogen Adsorption Capacity at 273, 288, and 298 K and Heat of Adsorption

sample code	adsorption capacity (cm^3/g)						Heat of adsorption (kJ/mol)	
	carbon dioxide			nitrogen			carbon dioxide	nitrogen
	273 K	288 K	298 K	273 K	288 K	298 K		
POP-1	37.7	29.2	26.4	3.0	2.7	2.2	39.1	13.1
POP-2	42.8	31.0	28.5	4.7	4.2	3.7	36.0	14.3
POP-3	51.7	40.5	32.5	4.9	4.5	3.5	32.6	15.2
POP-4	57.6	46.4	33.3	5.5	4.3	3.2	33.2	18.4

77 K (Table 1). The porosity of POP-3 and POP-4 is mostly made up of micropores (≤2 nm). POP-1 and POP-2 have comparatively, significantly low surface areas and pore volumes. The textural properties of the materials are listed in Table 1. It can be seen that the BET surface area and the total pore volume of the prepared materials are in the range of 22−585 m^2/g and 0.05−0.34 cm^3/g respectively. Snurr and co-workers[42,44] reported that the BET equation in the standard pressure range (0.05−0.3) may underestimate or overestimate the specific BET surface area for porous solids like zeolite and MOFs having pores of different dimensions. Applying the specific set of rules, the underestimation or overestimation of BET surface area could be minimized. Rouquerol and co-workers[43,45] suggested a set of rules known as consistency rules to overcome the BET limitations. Sinha et al.[46] also reported the limitations of the BET method. POP-1 and POP-2 successfully qualify the consistency rules with a positive BET constant in the standard BET relative pressure (P/P_0) range of 0.05−0.3. POP-3 and POP-4 give a negative BET constant (C) in the standard relative pressure (P/P_0) range of 0.05−0.3. The BET pressure points ($P/P_0 < 0.01$) for the POP-3 and POP-4 were judicially selected to get a positive BET constant. The high surface area and pore volume are due to the formation of pores with narrow PSD in the micropore region (Figure 6). The PSDs show an increase in micropore volume going from POP-1 to POP-4. The textural properties of porous polymer materials strongly depend on the precursor used. Naphthalene-derived POP-4 showed a relatively large surface area due to the fused ring systems and non-uniform alignment of the naphthalene repeating units.[41]

3.2. Carbon Dioxide, Nitrogen Adsorption Isotherm, and CO_2/N_2 IAST Selectivity. The adsorption/desorption isotherms at 273, 288, and 298 K and up to a pressure of 1 bar were generated for indole, pyrene, carbazole, and naphthalene-derived porous polymer materials. The CO_2/N_2 selectivity was determined using IAST and extended Langmuir model fitting of the adsorption isotherm data. The carbon dioxide heat of adsorption was measured for all the samples. The carbon dioxide, nitrogen adsorption capacities, and initial heat of adsorption are given in Table 2.

3.2.1. Indole-Derived Porous Polymer (POP-1). Figure 7 shows CO_2 and N_2 adsorption isotherms generated at 273, 288, and 298 K and up to 1 atm pressure for the porous polymer derived from indole. POP-1 shows an equilibrium carbon dioxide adsorption capacity of 37.7, 29.2, and 26.4, respectively, at 273, 288, and 298 K. The adsorption capacity for both carbon dioxide and nitrogen decreases with increasing adsorption temperatures. The adsorption/desorption isotherms are completely reversible. The decrease in adsorption capacity with increasing adsorption temperature and the reversible nature of the isotherm suggest the formation of weak interactions between the adsorbent and adsorbate gas molecules. The carbon dioxide and nitrogen adsorption on POP-1 is mostly due to the physisorption of gas molecules on the surface of the material. The CO_2/N_2 selectivity measured using IAST for the POP-1 is given in Figure 8. The selectivity is high in the low-pressure region and decreases with increasing pressure. However, it is interesting to note that this material shows higher selectivity at 298 K than selectivity at 273 and

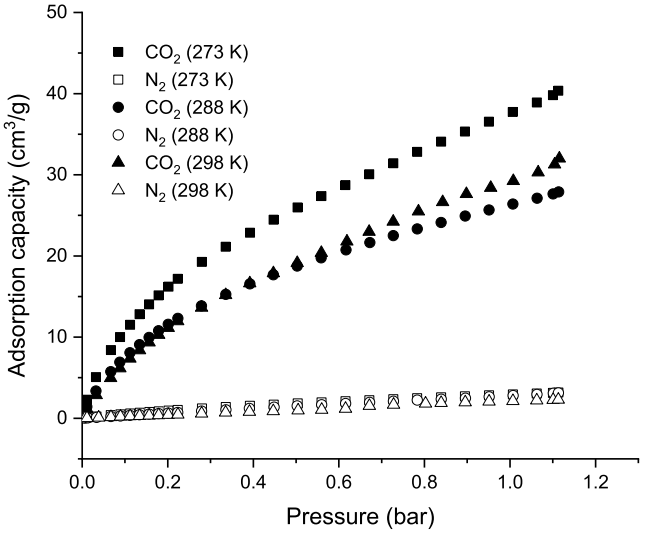

Figure 7. Carbon dioxide and nitrogen adsorption isotherms at 273, 288, and 298 K for POP-1.

https://doi.org/10.1021/acsomega.2c07553
ACS Omega 2023, 8, 24761−24772

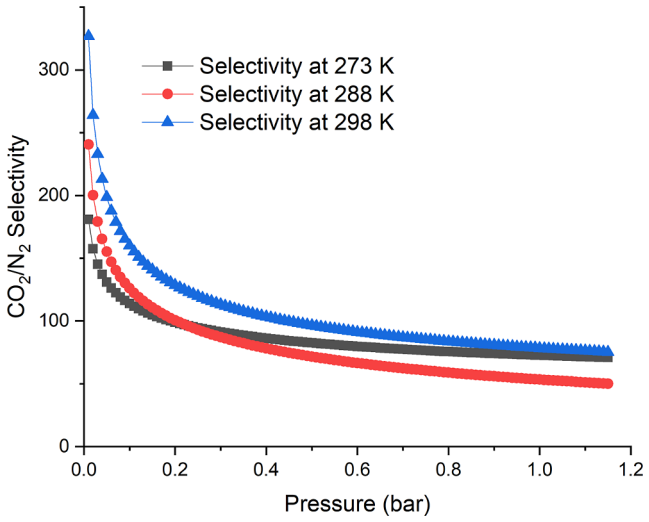

Figure 8. Carbon dioxide and nitrogen (CO_2/N_2: 15/85) adsorption selectivity at 273, 288, and 298 K for POP-1.

288 K. The relative atomic % of nitrogen for POP-1 is given in Table S1. The indole-derived POP-1 and carbazole-derived POP-3 have 9.28 and 6.72% nitrogen, respectively. A trace amount of chloride was also observed in the materials. Indole-derived POP-2 and naphthalene-derived POP-4 do not have nitrogen content. The N content generates basic sites in the material and favors the adsorption of acidic carbon dioxide molecules. This leads to higher carbon dioxide adsorption and low nitrogen adsorption in the low-pressure region. The increase in temperature favors CO_2 adsorption via acid−base interaction and decreases nitrogen adsorption via N−N repulsion. The POP-1 shows a better fit for dual-site extended Langmuir model fitting. This also indicates different adsorption mechanisms for carbon dioxide and nitrogen adsorption on POP-1.

Heteroatoms or functional groups on the surface of the porous polymer matrix have an immense effect on the adsorption capacity and selectivity. The effect of weak van der Waal forces and heteroatoms has also been distinctively studied to understand better adsorption capacity and selectivity. The N−carbon dioxide interactions are well studied in terms of their acid−base interactions as well as extended computational calculations like DFT and high-level wave function theory.[47] The increase in temperature favors CO_2 adsorption via acid−base interaction. This assumption of N−CO_2 interaction and enhanced initial CO_2 adsorption is indicated by the high CO_2/N_2 selectivity in the low-pressure region (Figure 8). The selectivity depends on the amount of CO_2 and N_2 adsorbed at specific temperatures and pressures. As expected, it was observed that the amount of both carbon dioxide and nitrogen adsorption via physical adsorption decreased with increasing temperature. However, in the low-pressure region, the % decrease in CO_2 adsorption is lower than the % decrease in N_2 adsorption. Wang et al.[48] also reported that the pore volumes from small pore sizes play an important role in carbon dioxide adsorption at 273 K, whereas surface chemistry is the key factor at a higher adsorption temperature or lower relative pressure. The acid−base interaction operates during initial adsorption (low-pressure region), and such interactions are favored at higher temperatures, i.e., 25 °C than 0 and 15 °C. Therefore, we assume that the high CO_2/N_2 selectivity in the low-pressure region increases with increasing temperature. Yang et al.[49] also reported increased mobility of gas molecules in the hyper-cross-linked porous materials. The pore flexibility among porous polymers increases the availability and diffusivity of gas molecules for interaction with N-active sites in the ultra-micropores of POP-1. Hao et al.[32] also reported that the high uptake at the initial stage of the adsorption isotherm in the nitrogen-containing porous carbon is attributed to the affinity between basic nitrogen groups and CO_2 via the acid−base interaction. Chiang et al.[41] also reported that high CO_2 adsorption on carbon nanofibers in the low-pressure region was attributed to the N-content of the material.[16,33] Simultaneously, the presence of nitrogen in POP-1 may decrease nitrogen adsorption due to the repulsion between nitrogen molecules and surface nitrogen. Rani and Dharamvir[34] reported N−N repulsions for nitrogen adsorption on graphene sheets. Wang et al.[35] compared the nitrogen adsorption energies of the two ccp-hcp sites on plutonium hydride and observed that the nitrogen atom exhibited slightly less preferred adsorption at the ortho hcp site. They interpreted this relationship by the repulsion of the two nitrogen atoms on the surface of the material. Panczyk et al.[36] also reported repulsive interactions between adsorbed nitrogen and the ruthenium surface. However, a more detailed investigation is required to support N−N interactions. The introduction of suitable heteroatoms like nitrogen in the polymer matrix help to create further chemical characteristics, such as electronegativity differences, which help to induce selectivity in the gas adsorption. Though the adsorption mechanism follows physisorption via weak van der Waals interactions, the induced dipole in the polymer matrix helps with selectivity as well as capacity in the gas adsorption.[20,23,31] The results show that taking into account the heterogeneity and hetero-chemistry present in porous materials is important to appropriately represent the adsorption capacity and selectivity of the porous polymeric materials at different temperatures and pressures. Electrostatic in-plane and dispersive $\pi-\pi$ stacking due to the aromatic rings also have an unavoidable effect on the adsorption selectivity. Therefore, the structural arrangement of aromatic rings, whether they are fused rings, directly linked, or flexible through a single bond to rotate, would immensely affect the polymer's textural properties (surface area, pore size, and pore volume). The in-plane conformations for different N-containing molecules are very different, and hence, the mere presence of nitrogen is not sufficient to achieve better selectivity in adsorption. The N-active site should also be accessible for gas molecules for the adsorption.

The IAST selectivity for a carbon dioxide-nitrogen gas mixture with typical flue gas composition (CO_2/N_2: 15/85) at 273, 288, and 298 K at 1 bar is 72.7, 53, and 78, respectively. This shows that the material shows excellent CO_2/N_2 selectivity at all the temperatures and pressures studied. Figure 8 shows very high selectivity in the low-pressure region. POP-1 shows CO_2/N_2 selectivity of 181, 241, and 327 at 273, 288, and 298 K, respectively, at 0.01 bar.

The heat of adsorption is a parameter to measure the strength of the interaction between carbon dioxide and the polymer surface. The heat of adsorption also suggests an affinity between the polymer surface and carbon dioxide molecules. The heat of adsorption also indicates the heterogeneity of the polymer surface for the adsorption of carbon dioxide and nitrogen gas molecules. The initial carbon

https://doi.org/10.1021/acsomega.2c07553
ACS Omega 2023, 8, 24761−24772

dioxide heat of adsorption for POP-1, POP-2, POP-3, and POP-4 is 39.1, 36.0, 32.6, and 33.2 kJ/mol, respectively. Among the studied samples, POP-1 shows the highest heat of adsorption for carbon dioxide and the lowest heat of adsorption for nitrogen adsorption. The high heat of adsorption for POP-1 is due to carbon dioxide adsorption via the acid−base interaction. However, the low heat of nitrogen adsorption is due to nitrogen adsorption via weak interactions and the repulsion of nitrogen gas molecules by surface nitrogen.

3.2.2. Pyrene-Derived Porous Polymer (POP-2). Figure 9 shows CO_2, and N_2 adsorption isotherms generated at 273, 288, and 298 K and up to 1 atm pressure for the porous polymer derived from pyrene. POP-2 shows equilibrium carbon dioxide adsorption capacities of 42.8, 31.0, and 28.5, respectively, at 273, 288, and 298 K. POP-2 shows nitrogen adsorption capacities of 4.7, 4.2, and 3.7, respectively, at 273, 288, and 298 K. The carbon dioxide and nitrogen adsorption on POP-2 is due to the physisorption of gas molecules on the surface of the material. The CO_2/N_2 selectivity for the POP-2 at different temperatures and pressures is given in Table 3 and Figure 10. For POP-2, the selectivity is high in low-pressure regions and decreases with increasing pressure. The POP-2 shows a good fit for both carbon dioxide and nitrogen for extended Langmuir model fitting. POP-1 and POP-2 have a large number of ultra-micropores where carbon dioxide adsorption occurs via a pore-filling mechanism, instead of surface adsorption. Therefore, Langmuir fitting failed for adsorption on POPO-1 and POP-2. The Langmuir model considers adsorption via monolayer formation on a homogenous surface. Extended-Langmuir considered the surface heterogeneity and equilibrium concentration of components on the adsorbent surface. The extended Langmuir model fitted well for the carbon dioxide and nitrogen adoption data for all four POP-1, POP-2, POP-3, and POP-4 samples. Langmuir and extended-Langmuir model fitting for POP-1 (Figures S7 and S3) and fitted statistics (Table S2) were given in the Supporting Information. Tables S3−S6 provide extended-Langmuir model fitting parameters for carbon dioxide and nitrogen adsorption on POP-1, POP-2, POP-3, and POP-4, respectively. While the Langmuir model fitting parameters for carbon dioxide and nitrogen adsorption on POP-1 are given in Table S7.

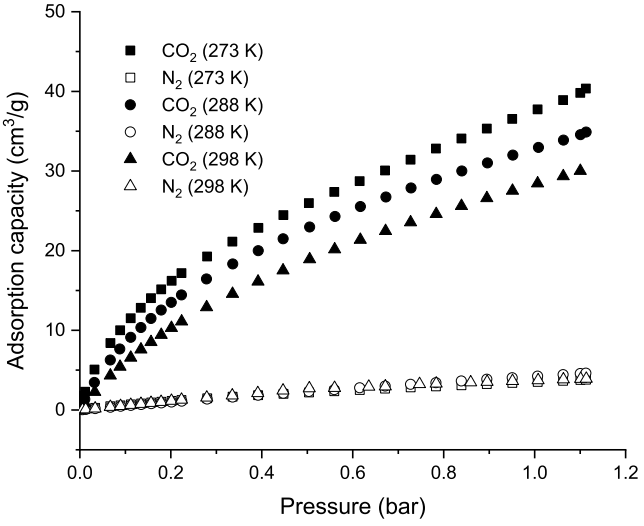

Figure 9. Carbon dioxide and nitrogen adsorption isotherms at 273, 288, and 298 K for POP-2.

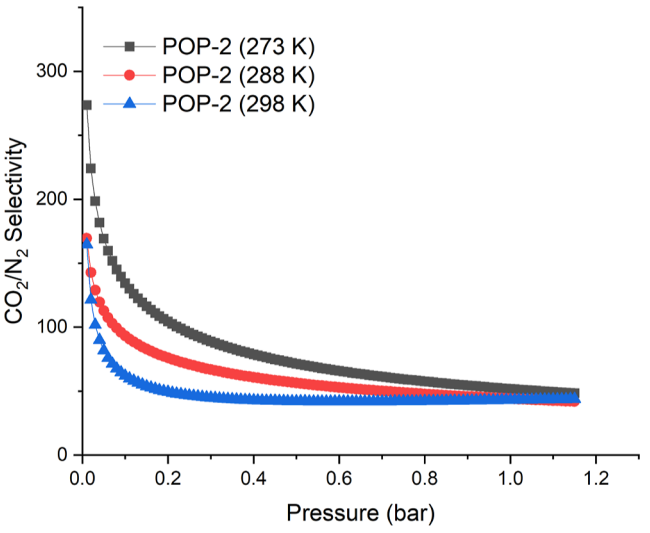

Figure 10. Carbon dioxide and nitrogen (CO_2/N_2: 15/85) adsorption selectivity at 273, 288, and 298 K for POP-2.

The IAST selectivity for a carbon dioxide-nitrogen gas mixture with typical flue gas composition (CO_2/N_2: 15/85) at 273, 288, and 298 K at 1 bar is 51.7, 44.1, and 43.1, respectively. IAST selectivity decreases with increasing pressure.

3.2.3. Carbazole-Derived Porous Polymer (POP-3). Figure 11 shows CO_2 and N_2 adsorption isotherms generated at 273, 288, and 298 K and up to 1 atm pressure for the porous polymer derived from carbazole (POP-3). POP-3 shows equilibrium carbon dioxide adsorption capacities of 51.7, 40.5, and 32.5, respectively, at 273, 288, and 298 K. POP-3 shows nitrogen adsorption capacities of 4.9, 4.5, and 3.5, respectively, at 273, 288, and 298 K. The CO_2/N_2 selectivity for POP-3 at different temperatures and pressures is given in Table 3 and Figure 12. Figure 3A indicates the EDX spectra for carbazole-derived porous POP-3. The POP-3 has 6.72%

Table 3. Carbon Dioxide and Nitrogen (CO_2/N_2: 15/85) Adsorption Selectivity at 273, 288, and 298 K

sample	IAST selectivity (CO_2/N_2: 15/85)								
	(pressure 0.01 bar)			(pressure 0.1 bar)			(pressure 1 bar)		
	273 K	288 K	298 K	273 K	288 K	298 K	273 K	288 K	298 K
POP-1	181.0	241.0	327.0	113.8	126.0	160.0	72.7	53.0	78.0
POP-2	273.5	169.4	164.6	134.4	93.3	62.1	51.7	44.1	43.1
POP-3	194	212.0	178	124.0	114.0	105.0	60.6	52.4	53.0
POP-4	215.2	165	124	127.3	106	101	60.0	59	56

https://doi.org/10.1021/acsomega.2c07553
ACS Omega 2023, 8, 24761−24772

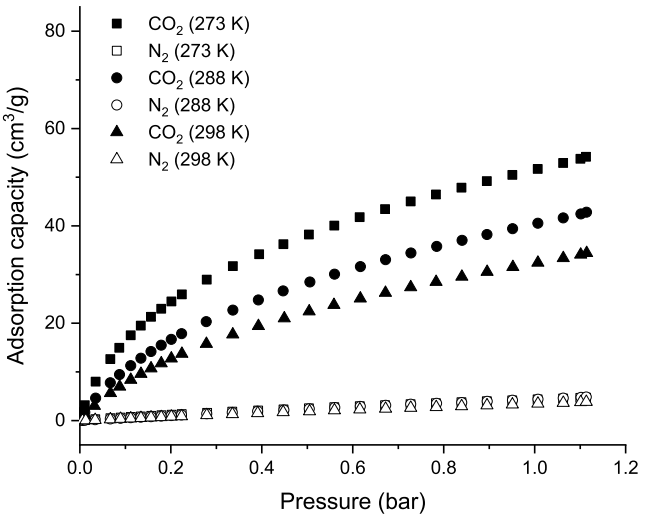

Figure 11. Carbon dioxide and nitrogen adsorption isotherms at 273, 288, and 298 K for POP-3.

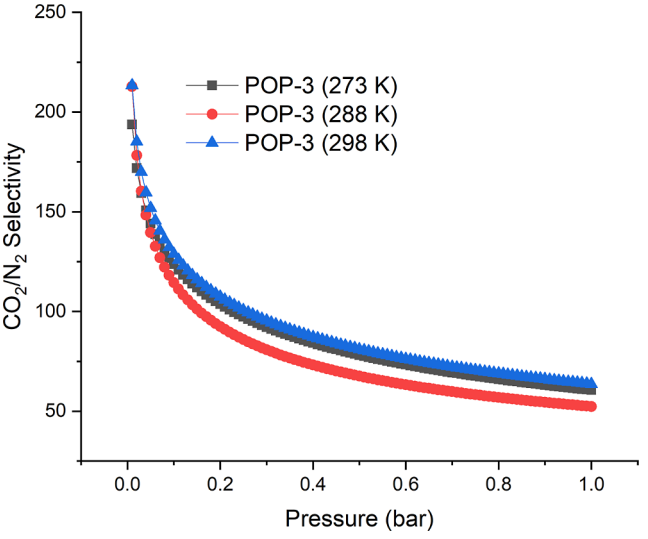

Figure 12. Carbon dioxide and nitrogen (CO_2/N_2: 15/85) adsorption selectivity at 273, 288, and 298 K for POP-3.

nitrogen. The N content generates basic sites in the material and leads to higher CO_2/N_2 selectivity in the low-pressure region. The POP-3 shows a good fit for both carbon dioxide and nitrogen for extended Langmuir model fitting. The IAST selectivity for a carbon dioxide−nitrogen gas mixture with typical flue gas composition (CO_2/N_2: 15/85) at 273, 288, and 298 K at 1 bar is 60.6, 52.4, and 53.0, respectively. IAST selectivity decreases with increasing pressure. POP-3 shows a surface area of 338 m^2/g, and a pore volume of 0.20 cm^3/g; the surface area and total pore volume of POP-3 are 16.2 and 4 times higher than POP-1, respectively, and 5.98 and 2.86 times higher than the surface area and pore volume of POP-2. Though POP-3 has a significantly higher surface area and pore volume, its carbon dioxide and nitrogen adsorption capacities are not that high in a similar ratio. This observation suggests the possible formation of ultra-micropores in POP-1 and POP-2, which are accessible to carbon dioxide and nitrogen gas molecules at ambient conditions but not to nitrogen gas molecules at 77 K.

3.2.4. Naphthalene-Derived Porous Polymer (POP-4). Figure 13 shows CO_2 and N_2 adsorption isotherms generated

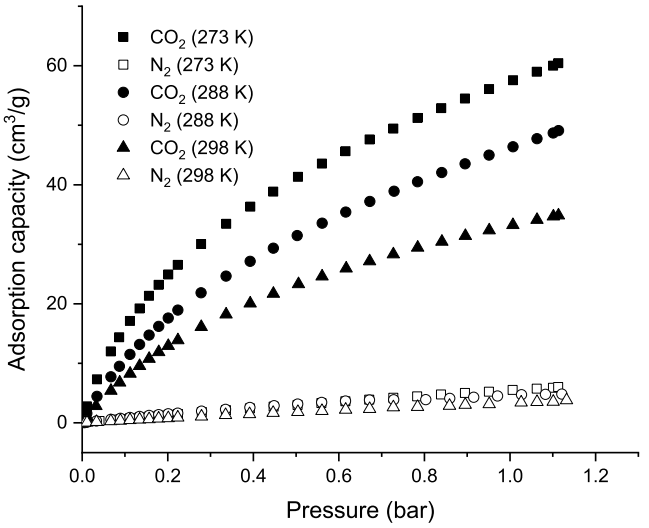

Figure 13. Carbon dioxide and nitrogen adsorption isotherms at 273, 288, and 298 K for POP-4.

at 273, 288, and 298 K and up to 1 atm pressure for the porous polymer derived from naphthalene. POP-4 shows equilibrium carbon dioxide adsorption capacities of 57.6, 46.4, and 33.3, respectively, at 273, 288, and 298 K. POP-4 shows nitrogen adsorption capacities of 5.5, 4.3, and 3.1, respectively, at 273, 288, and 298 K. The CO_2/N_2 selectivity for POP-4 at different temperatures and pressures is given in Table 3 and Figure 14.

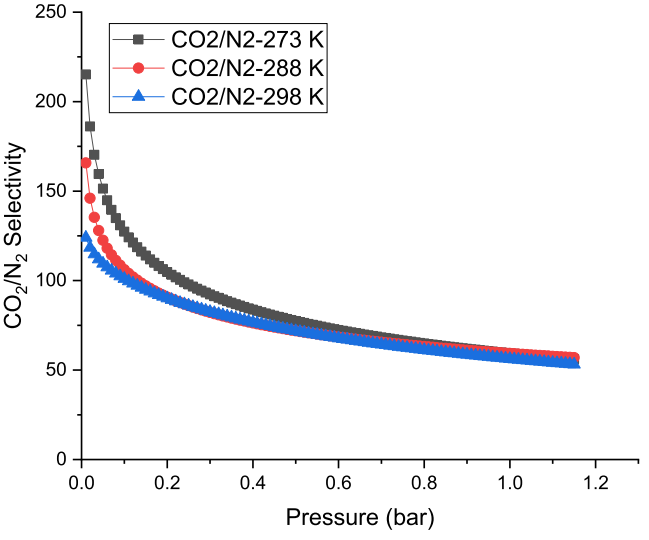

Figure 14. Carbon dioxide and nitrogen (CO_2/N_2: 15/85) adsorption selectivity at 273, 288, and 298 K for POP-4.

The selectivity is high in the low-pressure region and decreases with increasing pressure up to 1 bar. The nitrogen adsorption in POP-4 is not smooth and takes a long time to reach equilibrium. However, the isotherm is completely reversible. The POP-4 shows a good fit for both carbon dioxide and nitrogen for extended Langmuir model fitting. The IAST selectivity for a carbon dioxide-nitrogen gas mixture with typical flue gas composition (CO_2/N_2: 15/85) at 273, 288, and 298 K at 1 bar is 59.4, 57.6, and 60.1, respectively. IAST

https://doi.org/10.1021/acsomega.2c07553
ACS Omega 2023, 8, 24761−24772

selectivity decreases with increasing pressure. Naphthalene molecules possess extensive pi-bonding, and their molecular size is moderately smaller than the remaining precursors. The aromaticity is also much better than that of carbazole and indole, which are N-containing heterocycles. Therefore, the sliding ribbon-like polymers, as shown in Figure 15, would

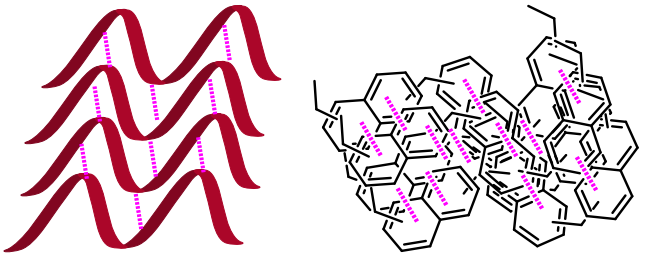

Figure 15. PHAPs derived from naphthalene showing $\pi-\pi$ stacking interactions.

have much better porosity to accommodate the CO_2 molecules.[30] However, the N-containing indole outperformed in the selectivity of CO_2 adsorption, which is due to the peculiar characteristic of the N-hetero atom present in the polymeric networks. In the case of carbazole, two phenyl rings flank the five-membered nitrogen-containing ring in, which the availability of nitrogen is very low compared to indole-derived POP-1.[50] The adsorption capacity and separation performance of the prepared materials under different conditions is compared with the carbon dioxide and nitrogen adsorption capacities and IAST selectivity of the adsorbents reported in the literature. Table S8 provided the comparison for carbon dioxide and nitrogen adsorption capacity (wt %) for different adsorbents at different pressures and 298 K. Table S9 provides the comparison for carbon dioxide and nitrogen adsorption capacities (mmol/g) at ambient temperature and pressure. POP-1 showed an INST selectivity of 78, which is higher than many of the reported adsorbents. POP-4 provides a balance of adsorption capacity and selectivity. However, the overall performance of the prepared adsorbents is less than that of the best-reported adsorbents. However, the material could be further tuned for higher capacity and selectivity. The adsorption capacity of POP-4 is also measured before and after 8 h of exposure to steam, carbon dioxide, and air (Figure S2). POP-4 showed excellent chemical and thermal stability under the experimental conditions, with about a 5% decrease in adsorption capacity after 8 h of exposure to steam, air, and carbon dioxide. POP-4 shows a decrease in surface area from 585 to 567 m^2/g after the treatment. To assess the suitability of the material for continuous use, 8 cycles of carbon dioxide adsorption/desorption measurements at 298 K were carried out. The POP-4 showed about a 3% decrease in carbon dioxide adsorption capacity after 8 cycles of carbon dioxide adsorption/desorption measurements (Figure S8).

4. CONCLUSIONS

A series of porous polymer materials with different porosities and compositions were prepared for the carbon dioxide and nitrogen separation. The decrease in adsorption capacity with increasing adsorption temperature and the reversible nature of adsorption/desorption isotherms suggest that the adsorption of carbon dioxide and nitrogen on these materials is governed by weak electrostatic interactions between the polymer and the carbon dioxide and nitrogen gas molecules. Among the prepared materials, POP-4 shows a maximum carbon dioxide adsorption capacity of 57.6 cm^3/g and a carbon dioxide/nitrogen selectivity of 60.0 at 273 K and 1 bar pressure. From the adsorption isotherm and model fit with the adsorption data, it is found that different mechanisms were simultaneously operated during the gas adsorption on the porous materials. Naphthalene-derived POP-4 possesses a higher surface area and pore volume with extensive pi-bonding and higher aromaticity with moderately smaller molecular size precursors than POP-1, POP-2, and POP-3. Therefore, POP-4 accommodates more CO_2 molecules. POP-1 shows higher CO_2/N_2 selectivity at 298 K than selectivity at 273 K and 288 K due to increased carbon dioxide adsorption via acid−base interaction and decreased nitrogen adsorption due to repulsion between surface nitrogen species and nitrogen gas molecules. The POP-1 shows a very high CO_2/N_2 selectivity of 327 in the low-pressure region. The high CO_2/N_2 selectivity for POP-1 is due to the peculiar characteristic of the N-hetero atom present in the polymeric networks. In the case of carbazole, two phenyl rings flank the five-membered nitrogen-containing ring, leading to a lower availability of nitrogen compared to indole-derived POP-1. The comparison of textural properties, composition, and gas adsorption properties for prepared materials suggests the role of surface area, pore volume, PSD, aromaticity, and N content. Further, fine-tuning of materials with desired properties may lead to superior adsorbents for carbon dioxide and nitrogen separation. The studied material could also be further doped with metal ions like sodium/lithium, which would help in achieving higher adsorption capacity and selectivity. The materials could also be functionalized or doped with N-containing species like PEI for higher adsorption capacity and selectivity. In the present study, we have not attempted the low molecular weight analog of naphthalene due to safety concerns; however, the analogs of benzene would be much more interesting for this kind of application. Integrating different approaches and methods can lead to superior materials with enhanced performance. The studies on the new POP samples prepared in the present series with micro- and mesoporosity and higher N-content are in progress.

■ ASSOCIATED CONTENT

Supporting Information

The Supporting Information is available free of charge at https://pubs.acs.org/doi/10.1021/acsomega.2c07553.

Schematic representation of experimental set-up, carbon dioxide adsorption isotherm before and after treatment, Langmuir and extended-Langmuir model fitting, repeated carbon dioxide adsorption/desorption cycles, EDX measurement, carbon dioxide adsorption capacity, and selectivity comparison (PDF)

■ AUTHOR INFORMATION

Corresponding Authors

Rajaram K. Nagarale − *Membrane Science and Separation Technology Division, Electro Membrane Processes Laboratory, CSIR-Central Salt and Marine Chemicals Research Institute, Bhavnagar 364002, India; Academy of Scientific and Innovative Research (AcSIR), Ghaziabad 201002, India;* orcid.org/0000-0002-9742-8104; Email: rkngarale@csmcri.res.in

https://doi.org/10.1021/acsomega.2c07553
ACS Omega 2023, 8, 24761−24772

Govind Sethia − *Inorganic Material and Catalysis Division, CSIR-Central Salt and Marine Chemicals Research Institute, Bhavnagar 364002 Gujarat, India; Academy of Scientific and Innovative Research (AcSIR), Ghaziabad 201002, India;* orcid.org/0000-0002-3979-4325; Email: govinds@csmcri.res.in

Authors

Noufal Merukan Chola − *Membrane Science and Separation Technology Division, Electro Membrane Processes Laboratory, CSIR-Central Salt and Marine Chemicals Research Institute, Bhavnagar 364002, India; Academy of Scientific and Innovative Research (AcSIR), Ghaziabad 201002, India*

Prayag Gajera − *Inorganic Material and Catalysis Division, CSIR-Central Salt and Marine Chemicals Research Institute, Bhavnagar 364002 Gujarat, India; Academy of Scientific and Innovative Research (AcSIR), Ghaziabad 201002, India*

Harshal Kulkarni − *Inorganic Material and Catalysis Division, CSIR-Central Salt and Marine Chemicals Research Institute, Bhavnagar 364002 Gujarat, India; Academy of Scientific and Innovative Research (AcSIR), Ghaziabad 201002, India*

Gaurav Kumar − *Inorganic Material and Catalysis Division, CSIR-Central Salt and Marine Chemicals Research Institute, Bhavnagar 364002 Gujarat, India; Academy of Scientific and Innovative Research (AcSIR), Ghaziabad 201002, India*

Rahulbhai Parmar − *Inorganic Material and Catalysis Division, CSIR-Central Salt and Marine Chemicals Research Institute, Bhavnagar 364002 Gujarat, India; Academy of Scientific and Innovative Research (AcSIR), Ghaziabad 201002, India*

Complete contact information is available at: https://pubs.acs.org/10.1021/acsomega.2c07553

Author Contributions

‖N.M.C., P.G. and H.K. contributed equally.

Notes

The authors declare no competing financial interest.

■ ACKNOWLEDGMENTS

The authors are thankful to the Science and Engineering Research Board (SERB), India, for financial support under project CVD/2021/000097 and the Council of Scientific and Industrial Research (CSIR) for financial support under project MLP-0054. The authors are thankful to the Centralized Instrumentation Facility of CSMCRI Bhavnagar for providing instrumentation facilities. CSIR-CSMCRI manuscript number 23/2023.

■ REFERENCES

(1) Earth's CO2 Home Page. https://www.co2.earth/ (accessed March 27, 2023).

(2) Samanta, A.; Zhao, A.; Shimizu, G. K. H.; Sarkar, P.; Gupta, R. Post-Combustion CO_2 Capture Using Solid Sorbents: A Review. *Ind. Eng. Chem. Res.* **2011**, *51*, 1438−1463.

(3) D'Alessandro, D. M.; Smit, B.; Long, J. R. Carbon Dioxide Capture: Prospects for New Materials. *Angew. Chem., Int. Ed.* **2010**, *49*, 6058−6082.

(4) Luo, R. C.; Chen, M.; Liu, X. Y.; Xu, W.; Li, J. Y.; Liu, B. Y.; Fang, Y. X. Recent advances in CO2 capture and simultaneous conversion into cyclic carbonates over porous organic polymers having accessible metal sites. *J. Mater. Chem. A* **2020**, *8*, 18408−18424.

(5) Kupgan, G.; Abbott, L. J.; Hart, K. E.; Colina, C. M. Modeling Amorphous Microporous Polymers for CO2 Capture and Separations. *Chem. Rev.* **2018**, *118*, 5488−5538.

(6) Sethia, G.; Sayari, A. Nitrogen-Doped Carbons: Remarkably Stable Materials for CO2 Capture. *Energy Fuels* **2014**, *28*, 2727−2731.

(7) Munusamy, K.; Sethia, G.; Patil, D. V.; Somayajulu Rallapalli, P. B.; Somani, R. S.; Bajaj, H. C. Sorption of carbon dioxide, methane, nitrogen and carbon monoxide on MIL-101(Cr): Volumetric measurements and dynamic adsorption studies. *Chem. Eng. J.* **2012**, *195−196*, 359−368.

(8) Jiang, Q. Y.; Rentschler, J.; Sethia, G.; Weinman, S.; Perrone, R.; Liu, K. L. Synthesis of T-type zeolite nanoparticles for the separation of CO2/N-2 and CO2/CH4 by adsorption process. *Chem. Eng. J.* **2013**, *230*, 380−388.

(9) Sethia, G.; Patel, H. A.; Pawar, R. R.; Bajaj, H. C. Porous synthetic hectorites for selective adsorption of carbon dioxide over nitrogen, methane, carbon monoxide and oxygen. *Appl. Clay Sci.* **2014**, *91−92*, 63−69.

(10) Sethia, G.; Sayari, A. Comprehensive study of ultra-microporous nitrogen-doped activated carbon for CO2 capture. *Carbon* **2015**, *93*, 68−80.

(11) Heydari-Gorji, A.; Belmabkhout, Y.; Sayari, A. Degradation of amine-supported CO_2 adsorbents in the presence of oxygen-containing gases. *Microporous Mesoporous Mater.* **2011**, *145*, 146−149.

(12) Meconi, G. M.; Tomovska, R.; Zangi, R. Adsorption of CO2 gas on graphene-polymer composites. *J. CO2 Util.* **2019**, *32*, 92−105.

(13) Shao, L. S.; Liu, M. Q.; Sang, Y. F.; Huang, J. H. One-pot synthesis of melamine-based porous polyamides for CO2 capture. *Microporous Mesoporous Mater.* **2019**, *285*, 105−111.

(14) (a) Tao, J.; Wang, Y. Y.; Tang, J. T.; Xiong, S. H.; Umar Javaid, M.; Li, G. H.; Sun, Q. M.; Liu, C.; Pan, C. Y.; Yu, G. P. Engineering pore surface and morphology of microporous organic polymers for improved affinity towards CO2. *Chem. Eng. J.* **2019**, *373*, 338−344. (b) Drage, T. C.; Snape, C. E.; Stevens, L. A.; Wood, J.; Wang, J.; Cooper, A. I.; Dawson, R.; Guo, X.; Satterley, C.; Irons, R. Materials challenges for the development of solid sorbents for post-combustion carbon capture. *J. Mater. Chem.* **2012**, *22*, 2815−2823. (c) Li, P.-Z.; Zhao, Y. Nitrogen-Rich Porous Adsorbents for CO_2 Capture and Storage. *Chem. Asian J.* **2013**, *8*, 1680−1691. (d) Wickramaratne, N. P.; Jaroniec, M. Importance of small micropores in CO2 capture by phenolic resin-based activated carbon spheres. *J. Mater. Chem. A* **2013**, *1*, 112−116. (e) Zhu, X.; Hillesheim, P. C.; Mahurin, S. M.; Wang, C.; Tian, C.; Brown, S.; Luo, H.; Veith, G. M.; Han, K. S.; Hagaman, E. W.; et al. Efficient CO_2 Capture by Porous, Nitrogen-Doped Carbonaceous Adsorbents Derived from Task-Specific Ionic Liquids. *ChemSusChem* **2012**, *5*, 1912−1917. (f) Zhang, Z.; Zhou, J.; Xing, W.; Xue, Q.; Yan, Z.; Zhuo, S.; Qiao, S. Z. Critical role of small micropores in high CO2 uptake. *Phys. Chem. Chem. Phys.* **2013**, *15*, 2523−2529.

(15) Sevilla, M.; Parra, J. B.; Fuertes, A. B. Assessment of the Role of Micropore Size and N-Doping in CO_2 Capture by Porous Carbons. *ACS Appl. Mater. Interfaces* **2013**, *5*, 6360−6368.

(16) Xing, W.; Liu, C.; Zhou, Z.; Zhang, L.; Zhou, J.; Zhuo, S.; Yan, Z.; Gao, H.; Wang, G.; Qiao, S. Z. Superior CO_2 uptake of N-doped activated carbon through hydrogen-bonding interaction. *Energy Environ. Sci.* **2012**, *5*, 7323−7327.

(17) (a) Dawson, R.; Cooper, A. I.; Adams, D. J. Chemical functionalization strategies for carbon dioxide capture in microporous organic polymers. *Polym. Int.* **2013**, *62*, 345−352. (b) Dawson, R.; Stöckel, E.; Holst, J. R.; Adams, D. J.; Cooper, A. I. Microporous organic polymers for carbon dioxide capture. *Energy Environ. Sci.* **2011**, *4*, 4239−4245. (c) Dawson, R.; Adams, D. J.; Cooper, A. I. Chemical tuning of CO2 sorption in robust nanoporous organic polymers. *Chem. Sci.* **2011**, *2*, 1173−1177.

(18) (a) Varghese, A. M.; Karanikolos, G. N. CO2 capture adsorbents functionalized by amine ? bearing polymers: A review. *Int. J. Greenhouse Gas Control* **2020**, *96*, 103005. (b) Mukhtar, A.; Saqib, S.; Mellon, N. B.; Babar, M.; Rafiq, S.; Ullah, S.; Bustam, M. A.; Al-Sehemi, A. G.; Muhammad, N.; Chawla, M. CO2 capturing,

thermo-kinetic principles, synthesis and amine functionalization of covalent organic polymers for CO2 separation from natural gas: A review. *J. Nat. Gas Sci. Eng.* **2020**, *77*, 103203.
(19) (a) Zou, L. F.; Sun, Y. J.; Che, S.; Yang, X. Y.; Wang, X.; Bosch, M.; Wang, Q.; Li, H.; Smith, M.; Yuan, S.; et al. Porous Organic Polymers for Post-Combustion Carbon Capture. *Adv. Mater.* **2017**, *29*, 1700229. (b) Huang, N.; Day, G.; Yang, X. Y.; Drake, H.; Zhou, H. C. Engineering porous organic polymers for carbon dioxide capture. *Sci. China: Chem.* **2017**, *60*, 1007−1014.
(20) Wang, W. J.; Zhou, M.; Yuan, D. Q. Carbon dioxide capture in amorphous porous organic polymers. *J. Mater. Chem. A* **2017**, *5*, 1334−1347.
(21) (a) Xu, C.; Hedin, N. Microporous adsorbents for CO2 capture - a case for microporous polymers? *Mater. Today* **2014**, *17*, 397−403. (b) Mason, J. A.; Sumida, K.; Herm, Z. R.; Krishna, R.; Long, J. R. Evaluating metal−organic frameworks for post-combustion carbon dioxide capture via temperature swing adsorption. *Energy Environ. Sci.* **2011**, *4*, 3030−3040. (c) Hedin, N.; Andersson, L.; Bergström, L.; Yan, J. Adsorbents for the post-combustion capture of CO2 using rapid temperature swing or vacuum swing adsorption. *Appl. Energy* **2013**, *104*, 418−433. (d) Ray, B.; Churipard, S. R.; Peter, S. C. An overview of the materials and methodologies for CO2 capture under humid conditions. *J. Mater. Chem. A* **2021**, *9*, 26498−26527.
(22) Errahali, M.; Gatti, G.; Tei, L.; Paul, G.; Rolla, G. A.; Canti, L.; Fraccarollo, A.; Cossi, M.; Comotti, A.; Sozzani, P.; et al. Microporous Hyper-Cross-Linked Aromatic Polymers Designed for Methane and Carbon Dioxide Adsorption. *J. Phys. Chem. C* **2014**, *118*, 28699−28710.
(23) Lu, X. Q.; Jin, D. L.; Wei, S. X.; Wang, Z. J.; An, C. H.; Guo, W. Y. Strategies to enhance CO2 capture and separation based on engineering absorbent materials. *J. Mater. Chem. A* **2015**, *3*, 12118−12132.
(24) Das, S.; Heasman, P.; Ben, T.; Qiu, S. Porous Organic Materials: Strategic Design and Structure−Function Correlation. *Chem. Rev.* **2017**, *117*, 1515−1563.
(25) Côté, A. P.; Benin, A. I.; Ockwig, N. W.; O'Keeffe, M.; Matzger, A. J.; Yaghi, O. M. Porous, Crystalline, Covalent Organic Frameworks. *Science* **2005**, *310*, 1166−1170.
(26) Dey, S.; Bhunia, A.; Esquivel, D.; Janiak, C. Covalent triazine-based frameworks (CTFs) from triptycene and fluorene motifs for CO2 adsorption. *J. Mater. Chem. A* **2016**, *4*, 6259−6263.
(27) Fan, H.; Mundstock, A.; Feldhoff, A.; Knebel, A.; Gu, J.; Meng, H.; Caro, J. Covalent Organic Framework−Covalent Organic Framework Bilayer Membranes for Highly Selective Gas Separation. *J. Am. Chem. Soc.* **2018**, *140*, 10094−10098.
(28) (a) Morris, J. R.; Contescu, C. I.; Chisholm, M. F.; Cooper, V. R.; Guo, J.; He, L.; Ihm, Y.; Mamontov, E.; Melnichenko, Y. B.; Olsen, R. J.; et al. Modern approaches to studying gas adsorption in nanoporous carbons. *J. Mater. Chem. A* **2013**, *1*, 9341−9350. (b) Wickramaratne, N. P.; Jaroniec, M. Activated Carbon Spheres for CO2 Adsorption. *ACS Appl. Mater. Interfaces* **2013**, *5*, 1849−1855.
(29) Tan, L.; Tan, B. Hypercrosslinked porous polymer materials: design, synthesis, and applications. *Chem. Soc. Rev.* **2017**, *46*, 3322−3356.
(30) Huang, J.; Turner, S. R. Hypercrosslinked Polymers: A Review. *Polym. Rev.* **2018**, *58*, 1−41.
(31) Borchardt, L.; Zhu, Q.-L.; Casco, M. E.; Berger, R.; Zhuang, X.; Kaskel, S.; Feng, X.; Xu, Q. Toward a molecular design of porous carbon materials. *Mater. Today* **2017**, *20*, 592−610.
(32) Hao, G. P.; Li, W. C.; Qian, D.; Lu, A. H. Rapid Synthesis of Nitrogen-Doped Porous Carbon Monolith for CO2 Capture. *Adv. Mater.* **2010**, *22*, 853−857.
(33) (a) Chiang, Y. C.; Lee, S. T.; Leo, Y. J.; Tseng, T. L. Importance of Pore Structure and Surface Chemistry in Carbon Dioxide Adsorption on Electrospun Carbon Nanofibers. *Sens. Mater.* **2020**, *32*, 2277−2288. (b) Sun, F.; Liu, X.; Gao, J.; Pi, X.; Wang, L.; Qu, Z.; Qin, Y. Highlighting the role of nitrogen doping in enhancing CO2 uptake onto carbon surfaces: a combined experimental and computational analysis. *J. Mater. Chem. A* **2016**, *4*, 18248−18252.
(34) Rani, B.; Dharamvir, K. A first principle study of adsorption of two proximate nitrogen atoms on graphene. *Int. J. Quantum Chem.* **2014**, *114*, 1619−1629.
(35) Wang, C. S.; Zhang, K.; Song, P.; Hu, X. F.; Mu, J. L.; Miao, Z. C.; Zhou, J.; He, H. First-Principles Study of Nitrogen Adsorption and Dissociation on PuH2 (111) Surface. *Molecules* **2020**, *25*, 1891.
(36) Panczyk, T. The influence of a small amount of active sites on the adsorption kinetics of nitrogen on ruthenium. *Appl. Surf. Sci.* **2005**, *252*, 687−698.
(37) Yang, X.; Yu, M.; Zhao, Y.; Zhang, C.; Wang, X.; Jiang, J.-X. Hypercrosslinked microporous polymers based on carbazole for gas storage and separation. *RSC Adv.* **2014**, *4*, 61051−61055.
(38) Puthiaraj, P.; Ahn, W.-S. CO2 Capture by Porous Hyper-Cross-Linked Aromatic Polymers Synthesized Using Tetrahedral Precursors. *Ind. Eng. Chem. Res.* **2016**, *55*, 7917−7923.
(39) Chola, N. M.; Nagarale, R. K. A Pseudocapacitor from Redox Active Covalent Organic Framework. *J. Electrochem. Soc.* **2021**, *168*, 100501.
(40) (a) Merukan Chola, N.; Nagarale, R. K. TCNQ Confined in Porous Organic Structure as Cathode for Aqueous Zinc Battery. *J. Electrochem. Soc.* **2020**, *167*, 100552. (b) Albers, P. W.; Leich, V.; Ramirez-Cuesta, A. J.; Cheng, Y.; Hönig, J.; Parker, S. F. The characterisation of commercial 2D carbons: graphene, graphene oxide and reduced graphene oxide. *Mater. Adv.* **2022**, *3*, 2810−2826.
(41) (a) Feng, J.; Zhang, Y.-J.; Ma, S.-H.; Yang, C.; Wang, Z.-P.; Ding, S.-Y.; Li, Y.; Wang, W. Fused-Ring-Linked Covalent Organic Frameworks. *J. Am. Chem. Soc.* **2022**, *144*, 6594−6603. (b) Ahmad, I.; Mahmood, J.; Baek, J.-B. Recent Progress in Porous Fused Aromatic Networks and Their Applications. *Small Sci.* **2021**, *1*, 2000007.
(42) (a) Gomez-Gualdron, D. A.; Moghadam, P. Z.; Hupp, J. T.; Farha, O. K.; Snurr, R. Q. Application of Consistency Criteria To Calculate BET Areas of Micro- And Mesoporous Metal-Organic Frameworks. *J. Am. Chem. Soc.* **2016**, *138*, 215−224. (b) Walton, K. S.; Snurr, R. Q. Applicability of the BET method for determining surface areas of microporous metal-organic frameworks. *J. Am. Chem. Soc.* **2007**, *129*, 8552−8556.
(43) Rouquerol, J.; Llewellyn, P.; Rouquerol, F. Is the BET Equation Applicable to Microporous Adsorbents? *Stud. Surf. Sci. Catal.* **2007**, *160*, 49−56.
(44) Bae, Y. S.; Yazaydin, A. O.; Snurr, R. Q. Evaluation of the BET Method for Determining Surface Areas of MOFs and Zeolites that Contain Ultra-Micropores. *Langmuir* **2010**, *26*, 5475−5483.
(45) Rouquerol, F.; Rouquerol, J.; Sing, K. S.; Llewellyn, P.; Maurin, G. *Adsorption by Powders and Porous Solids*; Elsevier Collection, 2014.
(46) Sinha, P.; Datar, A.; Jeong, C.; Deng, X.; Chung, Y. G.; Lin, L.-C. Surface Area Determination of Porous Materials Using the Brunauer−Emmett−Teller (BET) Method: Limitations and Improvements. *J. Phys. Chem. C* **2019**, *123*, 20195−20209.
(47) (a) Rochelle, G. T. Amine Scrubbing for CO_2 Capture. *Science* **2009**, *325*, 1652−1654. (b) Lee, H. M.; Youn, I. S.; Saleh, M.; Lee, J. W.; Kim, K. S. Interactions of CO2 with various functional molecules. *Phys. Chem. Chem. Phys.* **2015**, *17*, 10925−10933.
(48) Wang, E.-J.; Sui, Z.-Y.; Sun, Y.-N.; Ma, Z.; Han, B.-H. Effect of Porosity Parameters and Surface Chemistry on Carbon Dioxide Adsorption in Sulfur-Doped Porous Carbons. *Langmuir* **2018**, *34*, 6358−6366.
(49) Yang, Y.; Narayanan Nair, A. K.; Sun, S. Adsorption and Diffusion of Methane and Carbon Dioxide in Amorphous Regions of Cross-Linked Polyethylene: A Molecular Simulation Study. *Ind. Eng. Chem. Res.* **2019**, *58*, 8426−8436.
(50) (a) Lee, J. S. M.; Briggs, M. E.; Hasell, T.; Cooper, A. I. Hyperporous Carbons from Hypercrosslinked Polymers. *Adv. Mater.* **2016**, *28*, 9804. (b) Luo, Y.; Li, B.; Wang, W.; Wu, K.; Tan, B. Hypercrosslinked Aromatic Heterocyclic Microporous Polymers: A New Class of Highly Selective CO2 Capturing Materials. *Adv. Mater.* **2012**, *24*, 5703−5707.

https://doi.org/10.1021/acsomega.2c07553
ACS Omega 2023, 8, 24761−24772